

Transport of organelles by elastically coupled motor proteins

Deepak Bhat* and Manoj Gopalakrishnan†

Department of Physics, Indian Institute of Technology Madras, Chennai 600036, India

(Dated: January 11, 2019)

Motor-driven intracellular transport is a complex phenomenon where multiple motor proteins attached to a cargo are simultaneously engaged in pulling activity, often leading to tug-of-war and bidirectional motion. However, most mathematical and computational models ignore the details of the motor-cargo interaction. A few papers have studied more realistic models of cargo transport by including elastic motor-cargo coupling, but either restricts the number of motors and/or uses purely phenomenological forms for energy-dependent hopping rates. Here, we study a generic Model In which N motors are elastically coupled to a cargo, which itself is subject to thermal noise in the cytoplasm and an additional external applied force. The motor-hopping rates are chosen to satisfy detailed balance with respect to the energy of stretching. The master equation is converted to a linear Fokker-Planck equation (LFPE), which yields the average positions of the cargo and motors, as well as their fluctuations and correlation functions. We apply this formalism to two specific forms of the hopping rates. Analytical results are obtained for mean cargo velocity, diffusion coefficient and the average force experienced by each motor for arbitrary N , and compared with numerical simulations. The expansion procedure also allows us to quantify load-sharing features among the cargo-bound motors. In general, we observe significant deviations between analytical predictions based on LFPE and the corresponding numerical results, which suggests a prominent role for higher order corrections.

PACS numbers: 05.40.Fb, 05.40.-a, 87.16.Nn, 05.10.Gg

I. INTRODUCTION:

Numerous bioprocesses like contraction of muscles, spatial organization of various biomolecules inside cell and DNA replication are made possible by involvement of miniaturized workers called molecular motors [1, 2]. These are a class of proteins capable of accomplishing different types of mechanical work inside eukaryotic cells by continuous hydrolysis of adenosine-triphosphate (ATP) molecules. Dyneins and kinesins are two important families of motor proteins called porters, responsible mainly for transport of various intra-cellular organelles. These motor proteins perform directed motion on microtubule filaments, typically with speeds of a few hundred nm/s. Generally, dyneins move in retrograde direction while kinesins show anterograde motion. They also generate forces of few pN in order to drag and deliver different organelles from one place to other [1–4].

Motor driven cargo transport is complex phenomena due to involvement of multiple motor proteins in simulations pulling activity. Often, presence of motors of both the directionality leads to saltatory motion of cargoes [4–6]. In experiments, observation that the oppositely polar motors engage in tug-of-war suggested the direct interaction through pulling cargo on which they are bound [7]. In fact, in these experiments elongation of organelles is seen which is caused by tension generated during hauling mechanism. If the cargo is mechanically stiffer, both the teams of engaged motors experience an opposing load.

This results in reduced velocity and faster detachment of motors from the filament affecting the statistics such as mean transport time of the cargo on the filament, average distance covered etc. Therefore, it is crucial to understand how load exerted on a team of motors shared among the individuals. However, collective behavior of a set similar interacting motors attached on to a single cargo is so far not clearly understood. In order to probe this aspect, in a recent experimental study, motors were made to attach on to DNA scaffold with controlled separation between motors [8]. The velocity and the stall force of the DNA scaffold was found be affected by varying the spatial separation between the motors, which suggests the presence of interaction mediated by the linker DNA scaffold. The indication that the motors of the same directionality also interact is an important factor, as far as load sharing features of engaged motors and hence the statistics of the transport properties are concerned. While the exact form of interaction could be quite complex, development of simple tractable models based on simplified, but realistic interaction among the motors is desirable.

One of the theoretical studies motivated our work in this front was the model by Stukalin and Kolomeisky [9, 10] in which the mean velocity and diffusion coefficient were calculated for two interacting helicase motor proteins. An interesting observation in the model was that, the interaction between the motors can enhance the mean velocity of the coupled motors. The interaction energy surmised in this model increases linearly with the separation between motors on the track. However, in the case of intra-cellular transport, the motor proteins and motor-driven membranous organelles like endosomes, mitochondria etc. are soft molecules with stiffness typically

* deepak@physics.iitm.ac.in

† manojgopal@iitm.ac.in

of the order of a few pN/nm [1]. Since motor proteins exert forces of few pN on these organelles, the elastic nature of motor-cargo assembly is likely to be an influential factor. Unlike the model in [9, 10], the energy considered here increases quadratically with the separation between the motors and, the number of motors pulling the cargo are not restricted to two. Further, the organelles driven by these motors are under the influence of noisy thermal environment. Considering all these in to account, here we study the role of elastic interaction between cargo bound multiple motor proteins on the statistical properties of the intra-cellular transport.

In the last few years, several studies have appeared, based (mostly) on a Hookean spring-like interaction between motor and the cargo [11–17, 19]. In [11], along with elastic interaction among the motors, by assigning nonlinear force-velocity curve to different motors, average runlength of multiple motor driven cargo in the presence of external force is studied computationally at different motor stiffnesses. A more systematic semi-analytic study done by Materassi *et.al.* [12] reproduced the results in [11]. One of the major aspect in this type of model is that, motors experience a stochastic dynamic force, as the elastic force is determined by the instantaneous separation between the motor and the cargo [11, 13]. It was shown in [13] that, rather than "mean-field" model in which load is assumed to be shared equally among the motors of same directionality (see [20, 21] for details on "mean-field" model), stochastic load sharing model based on elastic motor-cargo interaction can explain unidirectional transport more reliably. They found, however, that both the models are not consistent with experimental observations of bidirectional transport. In another computational study, Bouzat and Falo [16] have shown that the stall force of the cargo motor assembly is larger for non-interacting motors than the motors interacting through elastic strain force. In [17], tug-of-war between multiple opposing motors is investigated and it was shown that the mean velocity of the cargo is independent of the stiffness, whereas the mean runtime decreases with such parameter. A discrete state transition rate model employed in [19] showed slight reduction in the two motor run length and velocity at larger stiffnesses, due to increase in the strain force. In a more recent study, Berger *et.al.* have identified distinct transport regimes in two elastically coupled motor proteins [14, 15]. Four regimes were identified by comparing strain force with the single motor stall force and the detachment force. Four other distinct regimes were found by comparing the time for spontaneous unbinding of motors from the filament with the time taken for motor-cargo system to build a force of the order of stall force and detachment force.

Some of the formalisms developed in above mentioned analytical studies are appropriate for at most two motor proteins driving a cargo [14, 15, 19], while many other studies are by and large computational in nature [11, 13, 16, 17]. Adopting elastic interaction among motor-cargo complex, so far, a general satisfactory analytical

approach has not been developed. Particularly, how the load sharing features are effected in the presence of elastic coupling is not clearly known. How stall force depends on the stiffness of the motor-cargo linkers is not clearly understood. Further, the effective diffusion coefficient of the motor-cargo system is likely to be different from free motor or cargo diffusion coefficient, and how this varies with number of motors on the cargo and elastic coupling is so far not known in detail. Our analytical work presented here addresses some of these issues more systematically.

In this paper, we study the motion of a cargo particle, bound to N motors through Hookean springs. We develop a generic formalism based on the well-known system size expansion, which separates systematically the average behavior from fluctuations. Because of its very nature, the formalism is suitable for arbitrary hopping rates and number of motors. Specifically, we consider two types of energy-dependent motor hopping rates (a) Glauber rates[22] $W_{\pm}(\Delta E) = W_{\pm}(0)/[1+\exp(\pm\Delta E)]$, although widely used in transport processes [23] which do not appear to have been used hitherto in literature in this context and (b) exponential rates of the form $W_+(\Delta E) = W_+(0)\exp(-\theta\Delta E)$, $W_-(\Delta E) = W_-(0)\exp((1-\theta)\Delta E)$ [9, 10, 24, 25] where ΔE is the energy difference between the original and target sites, measured in units of $\beta = (k_B T)^{-1}$ and θ is a parameter between 0 and 1, which is a measure of the underlying asymmetry in the energy landscape. We then make detailed comparisons between the predictions for the average velocity from both the models. Further, a systematic study of fluctuations in the force experienced by each motor and their mutual correlations is carried out. It is known that the detachment of motor is crucial for understanding the transport behavior [20, 21, 26]. However, we focus on average velocity, diffusion coefficient and force sharing features in this paper. To make the model simpler, we ignore the detachment of motors from the filament in our calculations here.

The paper is organized as follows: In section II, we discuss about the construction of master equation for cargo driven by multiple elastically coupled motor proteins, separation of dynamics of the averages in terms of a macroscopic equation and the dynamics of fluctuations about this average in terms of a Fokker-Planck equation. In section III, we present some of the results for cargo driven by N identical motor proteins within the model and compare these results with numerical simulations. Finally in section IV, we summarize our work with some discussion on the relevance, as well as limitations of the formalism.

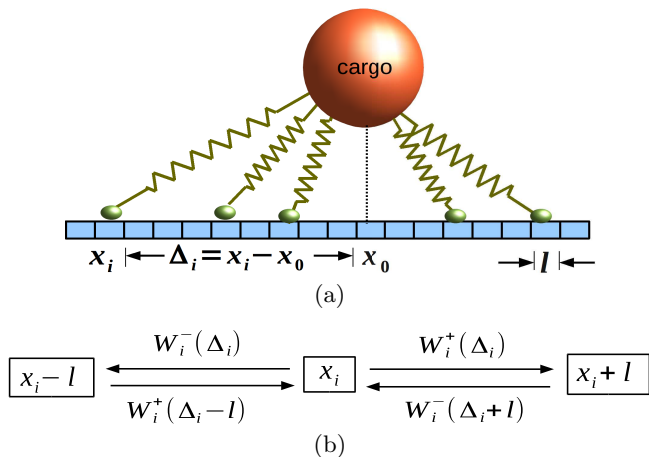


FIG. 1. (color online) (a) Cartoon of multiple elastic motor proteins (shown as springs) coupled through cargo performing Brownian motion on microtubule. (a) A motor at x_i jumps forward with a rate $W_i^+(\Delta_i)$ and backward with a rate $W_i^-(\Delta_i)$. Corresponding reverse transition rates from $x_i + \ell$ and $x_i - \ell$ are respectively given by $W_i^-(\Delta_i + \ell)$ and $W_i^+(\Delta_i - \ell)$.

II. MODEL AND THEORETICAL FORMALISM

A. Master Equation

A motor protein moving on a microtubule or actin filament moves in a sequence of jumps of fixed length from one monomer to the next (usually, although dynein is known to take variable-sized jumps in response to load [27, 28]). For a single free motor protein, let ℓ be the jump length and w_i and v_i be the forward and backward hopping rates respectively. A motor protein is imagined to be bound to the cargo using a spring of stiffness κ_i . We consider a cargo pulled by N such motor proteins simultaneously, as depicted in Fig.1(a). Let x_0 be the location of the cargo on the filament, and $x_i = \ell n_i$ ($1 \leq i \leq N$) be the locations of the motors (for simplicity, we ignore motor detachment in this paper). For the sake of later convenience, we use the convention $x \equiv \{x_0, x_1, \dots, x_N\}$. If $\Delta_i = x_i - x_0$ is the instantaneous separation between i 'th motor and the cargo, then the instantaneous elastic force on the i 'th motor and the cargo are, respectively, $f_i = -\kappa_i \Delta_i$ and $f_c = \sum_{n=1}^N \kappa_n \Delta_n$. For a cargo bound to N motor proteins and acted by an external force $-f$, the (over-damped) Langevin's equation may be written as [16]:

$$\dot{x}_0 = \sum_{n=1}^N \frac{\kappa_n \Delta_n}{\gamma} - \frac{f}{\gamma} + \zeta(t) \quad (1)$$

where γ is the drag coefficient, $\zeta(t)$ is Gaussian white noise: $\langle \zeta(t) \rangle = 0$ and $\langle \zeta(t) \zeta(t') \rangle = 2D \delta(t - t')$, where $D = k_B T / \gamma$ following fluctuation-dissipation theorem.

Let us denote by $W_i^+(\Delta_i)$ and $W_i^-(\Delta_i)$ the single motor hopping rates for the forward ($n_i \rightarrow n_i + 1$) and backward ($n_i \rightarrow n_i - 1$) transitions. Then the complete equation that describes the stochastic dynamics of the motor-cargo system may be written as

$$\begin{aligned} \frac{\partial P(x; t)}{\partial t} &= \sum_{i=1}^N [(\mathbb{E}_i^+ - 1)W_i^- P + (\mathbb{E}_i^- - 1)W_i^+ P] - \\ \frac{\partial}{\partial x_0} &\left[\left(\sum_{n=1}^N \frac{\kappa_n}{\gamma} \Delta_n - \frac{f}{\gamma} \right) P - D \frac{\partial P}{\partial x_0} \right] \end{aligned} \quad (2)$$

where \mathbb{E}_i^+ and \mathbb{E}_i^- are a set of N raising and lowering operators, defined through the relations $\mathbb{E}_i^+ f(n_1, n_2, \dots, n_i, \dots) = f(n_1, n_2, \dots, n_i + 1, \dots)$, and similarly, $\mathbb{E}_i^- f(n_1, n_2, \dots, n_i, \dots) = f(n_1, n_2, \dots, n_i - 1, \dots)$.

B. Fokker-Planck Equations

To proceed further, we will start with the following ansatz:

$$x_i = \bar{x}_i(t) + \eta_i \quad 0 \leq i \leq N \quad (3)$$

where $\bar{x}_i(t)$ are statistical averages, and therefore $\langle \eta_i \rangle = 0$. The dynamics may be entirely described now in terms of the variables η_i , the probability distribution of which is defined as $P(x, t) \equiv \Pi(\eta; t)$ so that

$$\frac{\partial P(x; t)}{\partial t} = \frac{\partial \Pi(\eta; t)}{\partial t} - \sum_{i=0}^N \frac{d\bar{x}_i}{dt} \frac{\partial \Pi}{\partial \eta_i} \quad (4)$$

The operators \mathbb{E}_i^+ and \mathbb{E}_i^- may be expanded as [18]

$$\mathbb{E}_i^\pm = 1 \pm \ell \frac{\partial}{\partial \eta_i} + \frac{\ell^2}{2} \frac{\partial^2}{\partial \eta_i^2} + \dots \quad (5)$$

Substitution of Eq.4 and Eq.5 into Eq.2 yields the following (non-linear) Fokker-Planck equation for the variables η_i :

$$\frac{\partial \Pi}{\partial t} = \sum_{i=0}^N \left[\dot{\bar{x}}_i \frac{\partial \Pi}{\partial \eta_i} - \frac{\partial}{\partial \eta_i} (V_i \Pi) + \frac{\partial^2}{\partial \eta_i^2} (D_i \Pi) + \mathcal{O}(\ell^3) \right] \quad (6)$$

where

$$V_i = \ell [W_i^+ - W_i^-] \quad ; \quad D_i = \frac{\ell^2}{2} [W_i^+ + W_i^-], \quad (7)$$

for $1 \leq i \leq N$, while

$$V_0 = \sum_{i=1}^N \frac{\kappa_i}{\gamma} \Delta_i - \frac{f}{\gamma} ; \quad D_0 = D \quad (8)$$

To proceed further, we will expand the rates also in the variables η_i , leading to

$$\begin{aligned} V_i(x) &= \bar{V}_i + \sum_j \alpha_{ij} \eta_j + \mathcal{O}(\eta^2) \\ D_i(x) &= \bar{D}_i + \sum_j \beta_{ij} \eta_j + \mathcal{O}(\eta^2), \end{aligned} \quad (9)$$

where we have defined the "macroscopic" variables

$$\bar{V}_i = V_i(\bar{x}) ; \quad \bar{D}_i = D_i(\bar{x}) \quad (10)$$

and the Taylor coefficients

$$\alpha_{ij} = \left. \frac{\partial V_i}{\partial \eta_j} \right|_{\eta=0} ; \quad \beta_{ij} = \left. \frac{\partial D_i}{\partial \eta_j} \right|_{\eta=0}. \quad (11)$$

Substitution of Eq.9 in Eq.6, and neglecting the β_{ij} terms (which do not contribute up to the second order moments in η_i) leads us to the linear Fokker-Planck equation

$$\begin{aligned} \frac{\partial \Pi}{\partial t} = \sum_{i=0}^N \left\{ \left(\dot{\bar{x}}_i - \bar{V}_i \right) \frac{\partial \Pi}{\partial \eta_i} + \bar{D}_i \frac{\partial^2 \Pi}{\partial \eta_i^2} - \right. \\ \left. \sum_{j=0}^N \alpha_{ij} \frac{\partial}{\partial \eta_i} (\eta_j \Pi) \right\} \end{aligned} \quad (12)$$

In order to satisfy the requirement that $\langle \eta_i \rangle = 0$, we put the convective terms in Eq.12 to zero, which yields the velocities

$$\dot{\bar{x}}_i = \bar{V}_i. \quad (13)$$

Also, by multiplying Eq.12 by $\eta_i \eta_j$ and integrating over all η , we obtain (see Appendix A for details) the following equations for the variances and correlations in η :

$$\frac{d}{dt} \langle \eta_i \eta_j \rangle = \sum_{n=0}^N 2\bar{D}_n \delta_{in} \delta_{jn} + \alpha_{in} \langle \eta_j \eta_n \rangle + \alpha_{jn} \langle \eta_i \eta_n \rangle \quad (14)$$

The results in Eq.13 and Eq.14 are valid for arbitrary number of motors of one or either directionality.

C. Energy dependence of motor hopping rates

We will now make specific choices for the functional form of motor hopping rates in the model, in such a way that the intrinsic asymmetry (essential for directed transport) in single motor rates is maintained, but the energy-dependence (corresponding to motor-cargo interaction) satisfies detailed balance. Let $E(x) = (1/2) \sum_i \kappa_i \Delta_i^2$ be the total energy of the system in a state $x \equiv \{x_0, x_1, \dots, x_i, \dots, x_N\}$. We define the local energy differences

$$\epsilon_i^\pm = \pm [E(\dots x_i \pm \ell, \dots) - E(\dots x_i, \dots)] = \frac{\kappa_i \ell}{2} [2\Delta_i \pm \ell] \quad (15)$$

for a certain motor i at position x_i , corresponding to a single hop to its right or left. Also, let w_i and $v_i \neq w_i$ be the intrinsic (asymmetric) forward and backward hopping rates respectively. Then, we surmise that the energy-dependent hopping rates introduced earlier follow a local detailed balance condition, i.e.,

$$\frac{W_i^+(\Delta_i)}{W_i^-(\Delta_i + \ell)} = \frac{w_i}{v_i} \exp(-\beta \epsilon_i^+) \quad (16)$$

with $\beta = (k_B T)^{-1}$. Note, however, that the dynamic quantities that characterize the transport process, e.g., the mean velocity of the cargo and its diffusion coefficient, depend on the difference and sum of the forward and backward rates respectively. Hence, our results for these quantities will depend on the specific forms for these rates, satisfying Eq.16. In the rest of this paper, we will consider two different forms:

Model I: Glauber rates

$$\begin{aligned} W_i^+(\Delta_i) &= \frac{w_i}{1 + \exp[\beta \epsilon_i^+]} \\ W_i^-(\Delta_i) &= \frac{v_i}{1 + \exp[-\beta \epsilon_i^-]} \end{aligned} \quad (17)$$

Model II: Asymmetric exponential rates

$$\begin{aligned} W_i^+(\Delta_i) &= w_i \exp[-\beta \epsilon_i^+ \theta_i] \\ W_i^-(\Delta_i) &= v_i \exp[\beta \epsilon_i^- (1 - \theta_i)] \quad (0 < \theta_i < 1) \end{aligned} \quad (18)$$

Model II has been studied in the literature [9, 10, 24, 25]. To the best of our knowledge, Model I with Glauber rates[22] has not been studied earlier in the context of motor proteins.

Eq.15-18 completes our development of the model. In the next section, we will extract analytical expressions for several quantities of interest for cargo driven by identical motors ($w_i = w, v_i = v, \kappa_i = \kappa, \theta_i = \theta$) using the formalism developed so far.

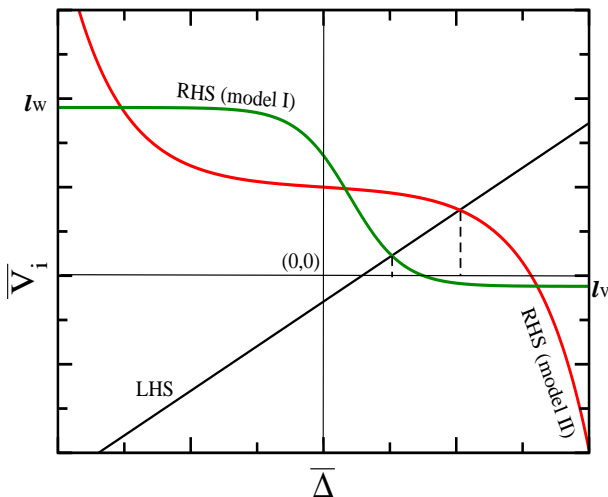


FIG. 2. (color online) The nature of curves in left hand side (LHS) and right hand side (RHS) of the Eq.20 is shown in this figure schematically. LHS is a straight line with slope $N\kappa/\gamma$. The RHS of the equation is shown for Model I and II separately. The solution to Eq.20 is $\bar{\Delta}$ for which LHS cuts the RHS in the figure (dashed line).

III. RESULTS

A. Average velocity and effective diffusion coefficient

(i) *Average cargo velocity.* For identical motors, since the hopping rates and stiffness of all the motors are equal, the mean separation between motor and the cargo is the same for all motors: $\bar{\Delta}_i \equiv \bar{\Delta}$. In this case, from Eq.8, the cargo velocity is

$$\bar{V}_0 = \frac{N\kappa}{\gamma}\bar{\Delta} - \frac{f}{\gamma}, \quad (19)$$

which implies that $\bar{\Delta}$ has to be non-zero in the long-time limit, and hence $\bar{V}_i = \bar{V}_0 \forall i \geq 1$ and $\bar{D}_i = \bar{D}_1 \forall i \geq 2$. Using Eq.7, Eq.10 and Eq.19, we thus arrive at the following transcendental equation for $\bar{\Delta}$:

$$\frac{N\kappa}{\gamma}\bar{\Delta} - \frac{f}{\gamma} = \ell [W^+(\bar{\Delta}) - W^-(\bar{\Delta})] \quad (20)$$

Let us look at this equation for simple case where external force on the cargo is zero ($f = 0$). The left hand side is a straight line with slope equal to $N\kappa/\gamma$ passing through origin. The right hand side is in general smooth monotonic function of $\bar{\Delta}$. It varies from ℓw to $-\ell v$ as $\bar{\Delta}$ is varied from $-\infty$ to ∞ in Model I (Eq.17) while in Model II (Eq.18), it varies from ∞ to $-\infty$ (see Fig.2 for schematic picture). Therefore, as slope $N\kappa/\gamma$ becomes larger and larger, the solution to the equation $\bar{\Delta}$ becomes smaller in magnitude (sign is positive if $w > v$ and negative if $w < v$). It suggests three different roles of

κ , γ and N respectively in the transport mechanism. (a) When γ becomes larger, cargo experiences a large drag force while motors try to pull it away. This increases the motor-cargo separation as γ increases. (b) As κ is increased, the energy cost due to stretching increases, larger separation between motor and cargo is energetically unfavorable and this will enhance the backward hopping rate of the motor. As a result, we see reduction in mean stretch $\bar{\Delta}$ with increase in κ (more details in next section). (c) Because all the motors are of same directionality, the number of springs which are connected in parallel increases (on an average) as N is increased. Due to additive nature of the spring constant in parallel springs, stretching of motors results in large energy cost and hence the mean separation between motor and cargo decreases with N . We will refer to these points again in subsequent sections where we use two different forms of rates given in Eq.17 and 18 explicitly.

(ii) *Effective diffusion coefficient:* Starting from Eq.14, the long time behavior of the variance $\langle \eta_i^2 \rangle$ can be calculated exactly for simple cases like $N = 1, 2$ (see Appendix A). In both these cases, the variance shows diffusive behavior in the long-time limit. For a general N motor system, we therefore expect $\langle \eta_i^2 \rangle \sim 2D_{\text{eff}}t$, where D_{eff} is the effective diffusion coefficient. Based on a simple extrapolation of the analytical results for $N = 1$ and 2 derived in Appendix A, we conjecture the following form for arbitrary N :

$$D_{\text{eff}} = \left[\frac{\alpha^2 D_0 + N \left(\frac{\kappa}{\gamma}\right)^2 \bar{D}_1}{\left(\alpha + N \frac{\kappa}{\gamma}\right)^2} \right] \quad (21)$$

where $\alpha \equiv \alpha_{10}$ and $\bar{D}_1 \equiv \bar{D}_n$ for $1 \leq n \leq N$. Eq.21 implies that $D_{\text{eff}} \propto N^{-1}$ as $N \rightarrow \infty$.

N dependence of \bar{V}_0 and D_{eff} : The asymptotic result above may be understood using an intuitive argument in the following way. For a free motor on the filament, w and v are forward and backward hopping rates respectively, with a fixed jump length ℓ . The average velocity and diffusion coefficient for this are given by $V_1 = \ell(w-v)$ and $D_1 = \ell^2(w+v)/2$ respectively. However, when multiple motor proteins are coupled through cargo, one may naively visualize whole system of motors as an effective random walker pulling a cargo with modified hopping rates ($w_e \sim Nw$ and $v_e \sim Nv$) and jump length ($\ell_e \sim \ell/N$). Then, the effective velocity $V_e = \ell_e(w_e - v_e)$ becomes independent of N while the effective diffusion coefficient $D_e = \ell_e^2(w_e + v_e)/2 \sim N^{-1}$ as $N \rightarrow \infty$. The scaling holds for a large range of stiffness, particularly when N is large. However, as discussed already, the exact effective velocity and diffusion coefficient depend on the effective stiffness ($\kappa_e = N\kappa$) in a highly nonlinear manner. This gives an additional weak N dependence to \bar{V}_0 and D_{eff} at small N , apart from the $1/N$ decay at large N .

(iii) *Average force and force-fluctuations:* To drag cargoes forward on the filament, the cargo-bound motors

have to overcome the backward viscous drag force on the cargo. In this competition, the elastic motor-cargo linker stretches, resulting in a backward force on the motors. Therefore, the average force on each motor will depend on the stiffness of the motor. (In the present study, all $\kappa_i = \kappa$, and hence the average force is same for all the motors). In the presence of external load f on the cargo, this also results in deviation of the instantaneous force experienced by a motor from the applied force per motor $-f/N$. It is interesting to understand how force exerted on the cargo is shared among the cargo-bound motors; in this context, it must be noted that both equal [20, 21] and stochastic [11, 13] load-sharing models of motor-protein transport have been studied in the literature. The present formalism allows us to characterize the statistics of force experienced per motor in a systematic way, within the constraints imposed by detailed balance.

The instantaneous force f_n on the n 'th motor is determined by the separation between the motor and cargo at that instant, i.e., $f_n = -\kappa(x_n - x_0) = -\kappa\Delta_n$. The expansion in Eq.3 allows us to write the average force experienced by the motor as $\langle f_n \rangle = -\kappa\bar{\Delta}$ for identical motors. To quantify the deviation of force experienced by the motor from f/N , we define $\delta f = f_n - (-f/N)$. From Eq.20, we notice an interesting relation between the average deviation in the force and the average cargo velocity, i.e.,

$$\langle \delta f \rangle = -\frac{\gamma\bar{V}_0}{N}, \quad (22)$$

which suggests that, when cargo is stalled ($\bar{V}_0 = 0$), then the deviation $\langle \delta f \rangle = 0$ (or $\langle f_n \rangle = -f/N$). Further, to study the statistics of fluctuations about $\langle \delta f \rangle$, the standard deviation is defined as $\sigma_f(N) = \sqrt{\langle \delta f^2 \rangle - \langle \delta f \rangle^2}$: it is easily shown that $\sigma_f^2 = \kappa^2[\langle \eta_n^2 \rangle + \langle \eta_0^2 \rangle - 2\langle \eta_0 \eta_n \rangle]$ for $n \geq 1$. From the expressions for $\langle \eta_p \eta_q \rangle$ (Appendix A), specific results for $N = 1$ and $N = 2$ are obtained:

$$\begin{aligned} \sigma_f(1) &= \kappa \sqrt{\left[\frac{D_0 + \bar{D}_1}{\alpha + \frac{\kappa}{\gamma}} \right]} \\ \sigma_f(2) &= \kappa \sqrt{\left[\frac{2D_0 + \bar{D}_1}{2(\alpha + 2\frac{\kappa}{\gamma})} + \frac{\bar{D}_1}{2\alpha} \right]}. \end{aligned} \quad (23)$$

(iv) *Stall force for a cargo pulled by N motors:* To determine the stall force f_s^N corresponding to vanishing cargo velocity, i.e., $\bar{V}_0 = 0$, we put the RHS of Eq.20 is equated to zero, the solution of which may be denoted $\Delta_s(\kappa)$. Then, from the LHS, the stall force is given by $f_s(\kappa) = N\kappa\Delta_s(\kappa)$. The exact expression for stall force in Model I turns out to be,

$$f_s^N = \frac{N}{\beta\ell} \log \left[\frac{y}{2} + \frac{1}{2} \sqrt{y^2 + 4\frac{w}{v}} \right] \quad (24)$$

where $y = (w - v) \exp(-\beta\kappa\ell^2/2)/v$. When $\kappa \simeq 0$, $y \simeq (w - v)/v$, and when $\kappa \rightarrow \infty$, $y \simeq 0$. Therefore, $f_s^N \approx N \log(w/v)/\beta\ell$ when $\kappa \rightarrow 0$ and $f_s^N \approx N \log(w/v)/2\beta\ell$ when $\kappa \rightarrow \infty$. That is, the stall-force decreases with the increase in κ and reaches half of its maximum value asymptotically. However, within Model II, the stall force behavior is different. Following the same procedure, we obtained the stall force here in Model II as follows:

$$f_s^N = N \left[\frac{1}{\beta\ell} \log \left(\frac{w}{v} \right) + \kappa\ell \left(\frac{1}{2} - \theta \right) \right] \quad (25)$$

We can see that as $\kappa \rightarrow 0$, stall force approaches an expected limit $f_s^N = N \log(w/v)/\beta\ell$ while f_s^N varies linearly as a function of κ with slope equal to $\ell(0.5 - \theta)$. If $\theta < 0.5$, the stall force increases with κ linearly. However, if $\theta > 0.5$ then, stall force decreases, it becomes zero at $\kappa = \log(w/v)/\beta\ell^2(0.5 - \theta)$ and then changes its sign above this stiffness. $\theta = 0.5$ seem to be a special case in which stall force does not depend on κ at all.

Numerical simulations, however, point to an entirely different situation: the stall force is found to be *independent* of κ , in both the models, at least in the range of κ studied here. This, and the other results from simulations, are presented in the next subsection.

B. Numerical simulations

Velocity versus κ : All the important results presented in the previous subsection were verified in computer simulations (Brownian dynamics for cargo motion, along with fixed time-step kinetic Monte-Carlo scheme for motor dynamics). We start with the forward and backward hopping rates given in Eq.17 and 18 separately. We have chosen the set of parameters given in Table.I, and found solution for $\bar{\Delta}$ from the transcendental equation 20 numerically. Then the mean cargo velocity \bar{V}_0 is evaluated from Eq.19. The results (dashed line) are shown for Model I and II in Fig.3(a) and Fig.3(b), respectively. As explained earlier, due to increase in energy cost for the movement of motors on the filament, average separation $\bar{\Delta}$ is reduced at larger κ . Therefore, the average velocity of the cargo decreases with κ as shown in the figure.

Increase in the number of motors results in a very small increase in the velocity at small κ , but the enhancement is negligibly small at large κ and large N . We can see these effects in both the models, shown in Fig.3. The analytical results show good agreement with simulations at small stiffness in both models. Deviation between the two at large stiffness indicates that the higher order terms in Eq.5 and 9 become important in this regime, more so in Model I than Model II. Even in Model II, deviations become significant at larger θ values (see Appendix B).

Diffusion coefficient versus κ : In the expression given in Eq. 21, κ -dependence of D_{eff} comes from α and \bar{D}_1 . Both the forward and backward decreases with κ , so \bar{D}_1

$w(s^{-1})$	$v(s^{-1})$	$\beta(pN^{-1}nm^{-1})$	$\gamma(pNs\ nm^{-1})$	$\ell(nm)$	θ
125.0028	0.0028	0.2433	9.42×10^{-4} [16]	8[29]	0.1[19]

TABLE I. (color online) A list of parameters used in the numerical simulations, with sources cited where required. Rates are chosen such a way that the velocity $V_1 = \ell(w - v)$ of the free motor becomes $1\mu ms^{-1}$.

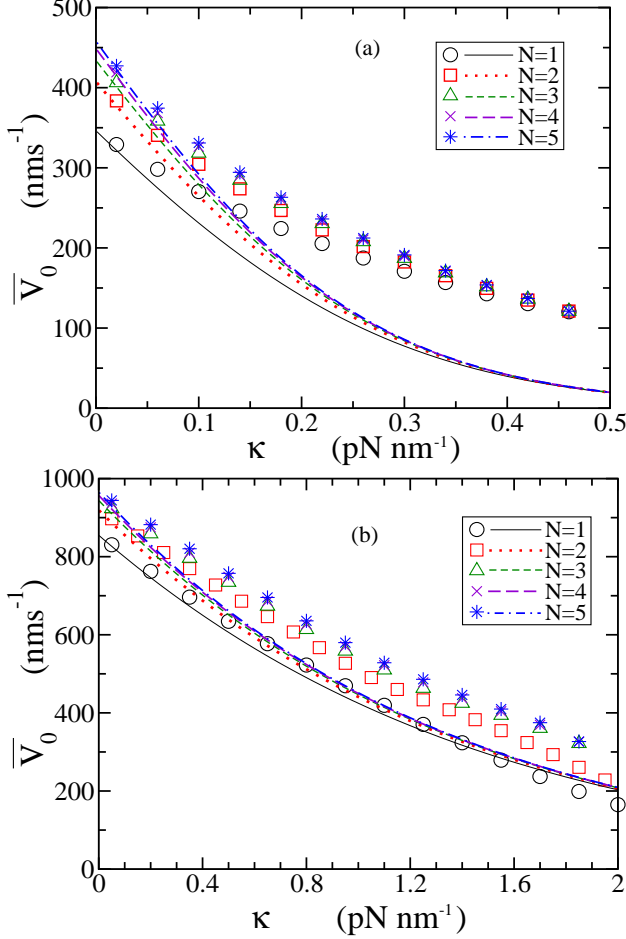


FIG. 3. (color online) Mean cargo velocity is shown as a function of stiffness at zero external force ($f = 0$), for different number of cargo bound motors. Figure (a) for Model I (Glauber rate) and (b) for Model II (asymmetric exponential rates). Dashed line is analytical result obtained from from Eq.19. Here in both (a) and (b), and also in subsequent plots the symbols are computer simulation results.

decreases accordingly. Moreover, α is also a decreasing function of κ . Therefore, as shown in Fig.4 (lines), effective diffusion coefficient D_{eff} (see Eq.21) of the motor cargo assembly, as predicted by theory, decreases with κ and should vanish asymptotically. Simulation results suggest, instead, that, D_{eff} also approaches a non-zero value as $\kappa \rightarrow \infty$. However, more simulations would be required to understand the large κ behavior of D_{eff} (and V_0) better.

The above results suggest that fluctuations about the

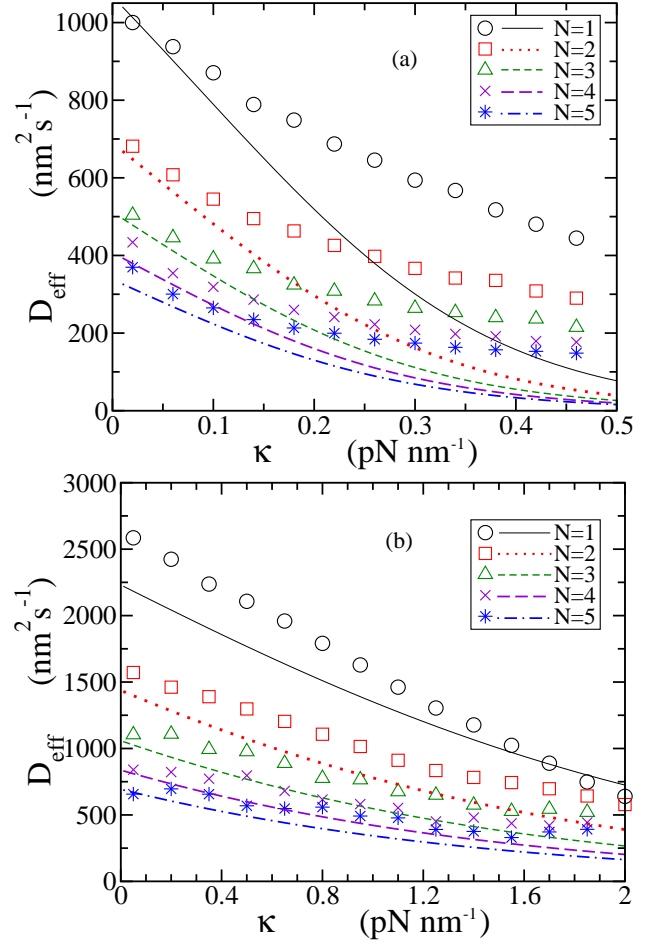


FIG. 4. (color online) The effective diffusion coefficient of the cargo as a function of stiffness for Model I in (a) and for Model II in (b). The diffusion coefficient varies inversely with number of motors on the cargo. Dashed line corresponds to Eq.21 and symbols are simulation results.

mean are suppressed by the increase in stretching energy cost at large stiffness. We also observe that D_{eff} reduces with increase in N (symbols in Fig.4), but the range of N studied in this paper is not sufficient to confirm the asymptotic power-law decay suggested by the theoretical calculations. We have seen Fig.3 that the velocity remains constant at larger motor numbers although it increases initially with N . Therefore, as N increases, multiple motor-mediated transport becomes more deterministic.

Load-sharing: In Fig.5 (a) and (b), the average force experienced by each motor $\langle f_n \rangle = -\kappa \bar{\Delta}_n$ is shown as a function of κ for Model I and II respectively. Even in the absence of external load on the cargo ($f = 0$), due to the backward viscous drag and elastic stretching by the forward movement of motors proteins, all the motors experience a net opposing force. Since, $\langle f_n \rangle = -\gamma \bar{V}_0 / N$ at $f = 0$, the decrease of $\langle f_n \rangle$ as a function of κ is related to the reduction in \bar{V}_0 with increasing stiffness. Further, with increase in number of motors, the force experienced

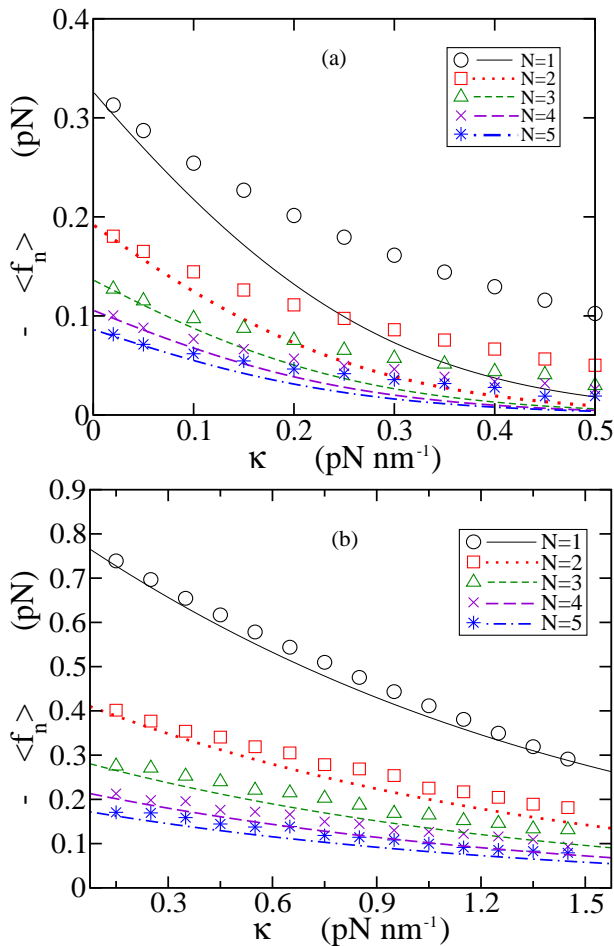


FIG. 5. (color online) The mean force experienced by each motor $\langle f_n \rangle = -\kappa \bar{\Delta}$ as a function of stiffness at $f = 0$ is shown here as dashed lines for Model I in (a) and II in (b). Symbols are computer simulation results.

by each motor motor also decreases as $1/N$, as expected.

Using Eq.22, we also looked at $\langle \delta f \rangle$, i.e., the deviation in the force experienced by the motor from f/N in the presence of an external force at fixed external force $f = 3$ pN. The deviation is found to be much smaller in Model I (Fig.6 (a)) compared to Model II (Fig.6 (b)). This is because, at $f = 3$ pN the velocity \bar{V}_0 itself becomes very much smaller for Model I compared that in Model II. The drastic reduction in velocity in Model I with increasing κ is associated with large changes in stretching energy, which suppress the hopping rates substantially.

Velocity versus f : In order to understand how velocity changes as a function of external force, we studied force-velocity curve for cargo driven by single motor ($N = 1$) at various stiffnesses for Model I and II, results are shown in Fig.7 (a) and (b) respectively. We see that, for the chosen set of parameters, the force-velocity curve is concave-up for Model I and convex-up for Model II (when $\theta = 0.1$). The origin of this difference may be understood using the following argument[2]. For a motor moving in plus direction, $\bar{\Delta} > 0$, and because of the form of the rate

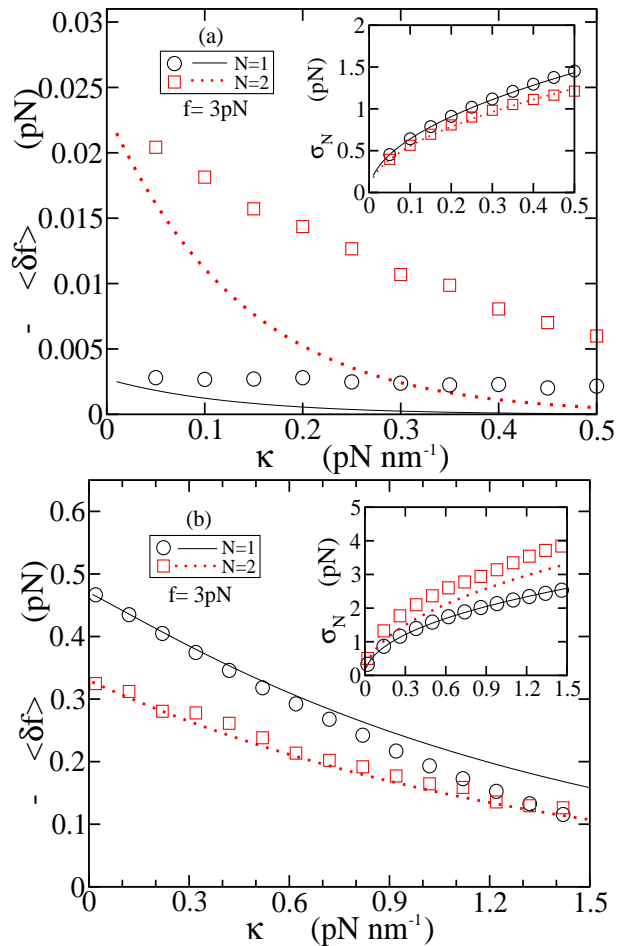


FIG. 6. (color online) The deviation from mean force experienced by each motor from f/N (Eq.22) is shown as a function of stiffness at $f = 3$ pN for Model I (a) and Model II (b). Inset shows Eq.19 as a function of κ . In both the figures, the symbols are computer simulation results.

in Model I, forward hopping of the motor by ℓ is exponentially suppressed while backward hopping occurs with intrinsic rate v . Therefore, force velocity curve is always concave up in this case. However, in Model II, the chosen load distribution factor $\theta (= 0.1)$ is less than 0.5; therefore, backward hopping rate is more sensitive to load. As a result, we see convex-up force velocity curve in this case. As shown in Fig.7 (a) and (b), qualitatively similar behavior is seen in computer simulations also. Nevertheless, a large deviation is observed at larger f in Model II, close to the regime where velocity becomes zero. In the simulations, the velocity becomes zero at same force for all κ values, indicating that the stall-force is independent of κ .

Stall force versus κ : To get more insights, we finally looked at stall-force $f_s^N(\kappa)$ as a function of κ for a cargo driven by varying numbers of motor proteins. For fast convergence, we replaced the constant force f with a harmonic trap force $f = -\kappa_t x$ where κ_t is the trap stiffness, with value chosen as 0.5 pN nm⁻¹. The results are shown

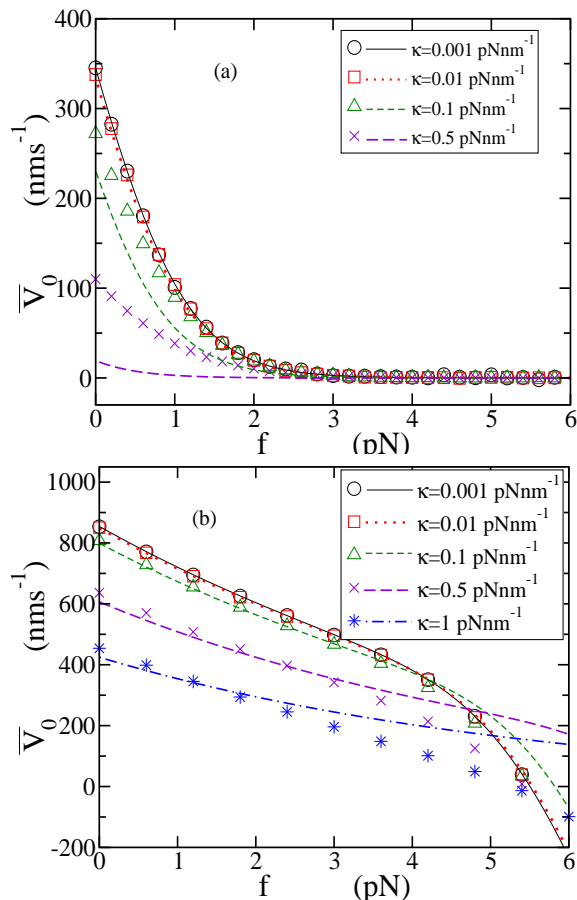


FIG. 7. (color online) Force-velocity curve is shown for cargo driven by a motor protein ($N = 1$) at different stiffnesses κ of the motor-cargo linker, for Model I in (a) and Model II in (b). Dashed line is from Eq.19 and symbols are simulation results.

in Fig.8 (a) and (b) for both Model I and II respectively. For Model I, Eq.24 predicts that the stall-force decreases with κ and approaches half of the maximum value (i.e., $f_s^N(0)$). In Model II, the theoretical prediction for the stall force expression is given by Eq.25, whose behavior as a function of κ was discussed in detail earlier: for $w > v$ and $\theta = 0.1$, stall force should increase linearly with κ . However, as found in numerical simulations, the stall force is, as much as observed, independent of κ in both the models (Fig.8 (a) and (b), symbols). We suspect that the underlying reason might lie in the existence of higher order terms in the expansion of the master equation, not captured in the LFPE approach pursued in this paper.

IV. SUMMARY AND CONCLUSIONS

Motor protein-driven cargo transport in eukaryotic cells is a complex and intriguing phenomenon due to the effective nonlinear interaction between bound motors on

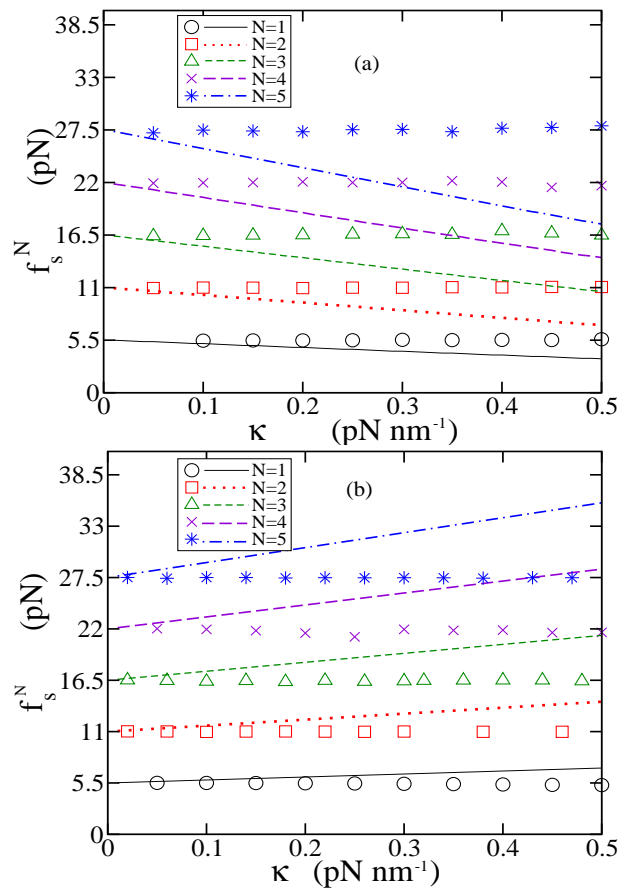


FIG. 8. (color online) Stall force as a function of stiffness κ for Model I in (a) and Model II in (b) is shown here. Dashed line corresponds to Eq.24 in (a) and Eq.25 in (b). The computer simulation results (symbols) suggests that stall force is independent of stiffness in Model II.

the cargo. The nonlinearity here arises from the elastic nature of the motor-cargo linkers. The effects of this elastic coupling on various aspects of cargo transport is only incompletely understood. This sets the background of our study here.

In the present model, motivated by many earlier studies, we regarded motor domains of these proteins as biased random walkers with fixed jump length, while the cargo subject, in addition to the elastic forces by motors, to thermal noise and an additional external force. Two models were used to describe the elastic energy dependence of the hopping rates, which we refer to as Model I and Model II. Model I uses Glauber-like dependence for elastic energy-dependence of hopping rates (Eq.17), while Model II uses asymmetric exponential rates (Eq.18). The master equation for the system is expanded to a linear Fokker-Planck equation (LFPE) using standard procedures [18, 30, 31]. The advantage of following this approach is that (a) it is a systematic and well-defined expansion, at least to the leading order [32], and (b) it can be employed for arbitrary forms of the hopping rates.

In the LFPE formalism, employing a transformation

of variables, the dynamical equations of the averages and fluctuations are separated systematically. By demanding that the average velocity of the motor and cargo are equal in the long time limit, a transcendental equation is obtained for mean motor-cargo separation. The solution to this equation yields various other quantities like the mean cargo velocity and average force experienced by the motor. By solving the Fokker-Planck equation for fluctuations, the effective diffusion coefficient is determined. It is shown that the mean cargo velocity becomes independent of motor number N while the diffusion coefficient vanishes asymptotically as $1/N$, for large N . Further, both the velocity and diffusion coefficient are found to decrease with increase in the stiffness of the motor-cargo linker. In the presence of an external load on the cargo, the average force experienced by the motor deviates from the load per motor because of the elastic coupling; the deviation is found to be more in Model II. This is a summary of the theoretical predictions.

When compared with numerical simulations, the formalism developed here gives very accurate results at small values of motor-cargo coupling stiffness (κ). Significant deviations are observed at larger κ , especially in Model I, where Glauber rates are used. We suspect that at high κ , higher order terms in the expansion of the master equation (beyond the linear noise approximation) play a major role. However, it must be emphasized that simulation results do agree qualitatively with analytical predictions in most cases. A serious limitation of the LFPE approach is observed in the estimation of stall-force as a function of κ at fixed N . While LFPE predicts a strong κ -dependence of the stall force in both models, simulations fail to show a similar effect. The reasons for the complete absence of any κ -dependence of stall force is not obvious to us, but its implications are clear; for instance, if found to be generally true, this results guarantees that the results for stall force measured for a motor using a glass bead as cargo in an *in vitro* optical trap experiment may be expected to be valid for a more flexible intracellular cargo also. The linear dependence of stall force on the number of motors N , another prediction in the model, is supported by simulations.

Recent experiments on transport of DNA-scaffold by motors with controlled separation between them, have thrown light on the possibility of motor-motor interactions during the transport [8]. In such experiments, it may be possible to test some of our predictions. We hope that the tools developed here will stimulate further interest in understanding how multiple motors coordinate themselves during an intra-cellular transport, and the role of elasticity of the cargo-motor complex in such processes.

ACKNOWLEDGMENTS

The authors would like to thank P.G. Senapathy Centre for Computing Resources, IIT Madras for computa-

tional support.

Appendix A: Derivation of effective diffusion coefficient for identical motors:

Due to the condition in Eq.13, the Fokker-Planck equation given in Eq.12 takes the following form:

$$\frac{\partial \Pi}{\partial t} = \sum_{n=0}^N \left[\overline{D}_n \frac{\partial^2 \Pi}{\partial \eta_n^2} - \sum_{m=0}^N \alpha_{nm} \frac{\partial}{\partial \eta_n} (\eta_m \Pi) \right] \quad (\text{A1})$$

We define the Fourier transform of Π with respect the variables η as:

$$\phi(g_0, g_1 \dots) = \int \exp[i(g_0 \eta_0 + g_1 \eta_1 + \dots)] \Pi(\eta_0, \eta_1 \dots) d\eta_0 d\eta_1 \dots \quad (\text{A2})$$

Using standard properties of the Fourier transform, the Eq.A1 may be re-written as follows:

$$\frac{\partial \phi}{\partial t} = \sum_{n=0}^N \left[-g_n^2 \overline{D}_n \phi + \sum_{m=0}^N \alpha_{nm} g_n \frac{\partial \phi}{\partial g_m} \right] \quad (\text{A3})$$

Next, we use the properties

$$\begin{aligned} \langle \eta_p \rangle &= \left. \frac{\partial \phi}{\partial (i g_p)} \right|_{g=0} \\ \langle \eta_p \eta_q \rangle &= \left. \frac{\partial^2 \phi}{\partial (i g_p) \partial (i g_q)} \right|_{g=0} \end{aligned} \quad (\text{A4})$$

to arrive at the equations

$$\frac{d}{dt} \langle \eta_p \rangle = \sum_{n=0}^N \alpha_{pn} \langle \eta_n \rangle \quad (\text{A5})$$

and

$$\begin{aligned} \frac{d}{dt} \langle \eta_p \eta_q \rangle &= \sum_{n=0}^N \left[2 \overline{D}_n \delta_{pn} \delta_{qn} + \alpha_{pn} \langle \eta_q \eta_n \rangle + \right. \\ &\quad \left. \alpha_{qn} \langle \eta_p \eta_n \rangle \right]. \end{aligned} \quad (\text{A6})$$

For identical motors, $\alpha_{00} = -N\alpha_{0m} = -N\frac{\kappa}{\gamma}$ ($m \geq 1$) and $\alpha_{nm} = -\alpha_{n0} = \alpha$ ($m, n \geq 1$). Note that $\alpha > 0$ and its actual value depends on the choice of rates in the Eq.2 and Eq.3 of main draft. Further, we have used the equality $\overline{D}_n = \overline{D}_1$ for $n \geq 1$. The lack of a non-homogeneous term in Eq.A5 ensures that $\langle \eta_p \rangle = 0$ in the steady state. From Eq.A6, we find time evolution of second moments for $N = 1$ as follows:

$$\begin{aligned}
\frac{d}{dt}\langle\eta_0^2\rangle &= 2D_0 + 2\frac{\kappa}{\gamma} [\langle\eta_0\eta_1\rangle - \langle\eta_0^2\rangle] \\
\frac{d}{dt}\langle\eta_1^2\rangle &= 2\overline{D}_1 + 2\alpha [\langle\eta_0\eta_1\rangle - \langle\eta_1^2\rangle] \\
\frac{d}{dt}\langle\eta_0\eta_1\rangle &= \alpha\langle\eta_0^2\rangle + \frac{\kappa}{\gamma}\langle\eta_1^2\rangle - \left(\alpha + \frac{\kappa}{\gamma}\right)\langle\eta_0\eta_1\rangle \quad (\text{A7})
\end{aligned}$$

To solve the above equations, we define the Laplace transforms $\langle\eta_p\eta_q\rangle_s = \int_0^\infty \exp(-st)\langle\eta_p\eta_q\rangle dt$. Eq.A7 is now expressed in matrix form and solved for the moments in Laplace space. For $N = 1$, the solution is

$$\begin{aligned}
\langle\eta_0^2\rangle_s &= \frac{2 \left[D_0 s^2 + D_0 (3\alpha + \frac{\kappa}{\gamma}) s + 2\alpha^2 D_0 + 2(\frac{\kappa}{\gamma})^2 \overline{D}_1 \right]}{s^2 (s + \alpha + \frac{\kappa}{\gamma}) (s + 2\alpha + 2\frac{\kappa}{\gamma})} \\
\langle\eta_1^2\rangle_s &= \frac{2 \left[\overline{D}_1 s^2 + \overline{D}_1 (\alpha + 3\frac{\kappa}{\gamma}) s + 2\alpha^2 D_0 + 2(\frac{\kappa}{\gamma})^2 \overline{D}_1 \right]}{s^2 (s + \alpha + \frac{\kappa}{\gamma}) (s + 2\alpha + 2\frac{\kappa}{\gamma})} \\
\langle\eta_0\eta_1\rangle_s &= \frac{2 \left[(D_0 \alpha + \overline{D}_1 \frac{\kappa}{\gamma}) s + 2\alpha^2 D_0 + 2(\frac{\kappa}{\gamma})^2 \overline{D}_1 \right]}{s^2 (s + \alpha + \frac{\kappa}{\gamma}) (s + 2\alpha + 2\frac{\kappa}{\gamma})}. \quad (\text{A8})
\end{aligned}$$

We observe that as $s \rightarrow 0$, $\langle\eta_0^2\rangle_s = \langle\eta_1^2\rangle_s = \langle\eta_0\eta_1\rangle_s \approx 2D_{\text{eff}}/s^2$, and hence $\langle\eta_0^2\rangle = \langle\eta_1^2\rangle = \langle\eta_0\eta_1\rangle \approx 2D_{\text{eff}}t$ where D_{eff} is the effective one-dimensional diffusion coefficient of the cargo on the filament, given by

$$D_{\text{eff}} = \left[\frac{\alpha^2 D_0 + (\frac{\kappa}{\gamma})^2 \overline{D}_1}{(\alpha + \frac{\kappa}{\gamma})^2} \right]. \quad (N = 1) \quad (\text{A9})$$

For $N = 2$, a similar analysis gives the moment-transforms

$$\begin{aligned}
\langle\eta_0^2\rangle_s &= \frac{2D_0 s^2 + 2D_0 (3\alpha + 2\frac{\kappa}{\gamma}) s + 4\alpha^2 D_0 + 8\overline{D}_1 (\frac{\kappa}{\gamma})^2}{s^2 (s + \alpha + 2\frac{\kappa}{\gamma}) (s + 2\alpha + 4\frac{\kappa}{\gamma})} \\
\langle\eta_1^2\rangle_s = \langle\eta_2^2\rangle_s &= \frac{2\overline{D}_1 s^3 + \overline{D}_1 (2\frac{\kappa}{\gamma} + \alpha) s^2 + 4[\alpha^2 (D_0 + \overline{D}_1) + 4(\frac{\kappa}{\gamma})^2 \overline{D}_1 + 3\alpha(\frac{\kappa}{\gamma}) \overline{D}_1] s + 8\alpha^3 D_0 + 16\alpha \overline{D}_1 (\frac{\kappa}{\gamma})^2}{s^2 (s + 2\alpha) (s + \alpha + 2\frac{\kappa}{\gamma}) (s + 2\alpha + 4\frac{\kappa}{\gamma})} \\
\langle\eta_0\eta_1\rangle_s = \langle\eta_0\eta_2\rangle_s &= \frac{2 \left[(\alpha D_0 + \overline{D}_1 \frac{\kappa}{\gamma}) s + 2\alpha^2 D_0 + 4(\frac{\kappa}{\gamma})^2 \overline{D}_1 \right]}{s^2 (s + \alpha + 2\frac{\kappa}{\gamma}) (s + 2\alpha + 4\frac{\kappa}{\gamma})} \\
\langle\eta_1\eta_2\rangle_s &= \frac{4\alpha \left[(\alpha D_0 + \overline{D}_1 \frac{\kappa}{\gamma}) s + 2\alpha^2 D_0 + 4(\frac{\kappa}{\gamma})^2 \overline{D}_1 \right]}{s^2 (s + 2\alpha) (s + \alpha + 2\frac{\kappa}{\gamma}) (s + 2\alpha + 4\frac{\kappa}{\gamma})}. \quad (\text{A10})
\end{aligned}$$

Similar to the previous case, it is easily shown that $\langle\eta_0^2\rangle = \langle\eta_1^2\rangle = \langle\eta_0\eta_1\rangle \approx 2D_{\text{eff}}t$ where

$$D_{\text{eff}} = \left[\frac{\alpha^2 D_0 + 2(\frac{\kappa}{\gamma})^2 \overline{D}_1}{(\alpha + 2\frac{\kappa}{\gamma})^2} \right]. \quad (N = 2) \quad (\text{A11})$$

Both Eq.A9 and Eq.A11 are combined in the expression for effective diffusion coefficient is given in Eq.21, which we conjecture to be valid for all N .

Eq.A8 and Eq.A10 allow us to find the mean-squared fluctuations (σ_f^2) about the deviation of the instantaneous force $\langle f_n \rangle$ experienced by a single motor from mean applied force f/N per motor. To find this, one need to

evaluate $\sigma_f^2 = \langle \delta f^2 \rangle - \langle \delta f \rangle^2 = \ell [\langle \eta_n^2 \rangle + \langle \eta_0^2 \rangle - 2\langle \eta_0 \eta_n \rangle]$. The expressions derived for $N = 1$ and $N = 2$ may be found in Eq.23.

Appendix B: \overline{V}_0 and D_{eff} at $\theta = 0.9$ for Model II

Here, for the sake of comparison with the $\theta = 0.1$ results in the main text, we give results for higher value of θ , i.e., $\theta = 0.9$. Fig.9 displays the results for the mean cargo velocity and diffusion coefficient as function of stiffness κ , for N in the range 1–5. Qualitatively, both analytical results from LFPE and simulations follow similar trends, but unlike the $\theta = 0.1$ case, the deviations between the two are significant here. Furthermore, the velocity-force curve is convex rather than concave.

[1] J. Howard *Mechanics of Motor Proteins and Cytoskeleton*, (Sinauer Press, Sunderland, MA 2001).

[2] R. Phillips, J. Kondev, J. Theriot and N. Orme, *Physical Biology of the Cell*, (Garland Science, New York, 2009).

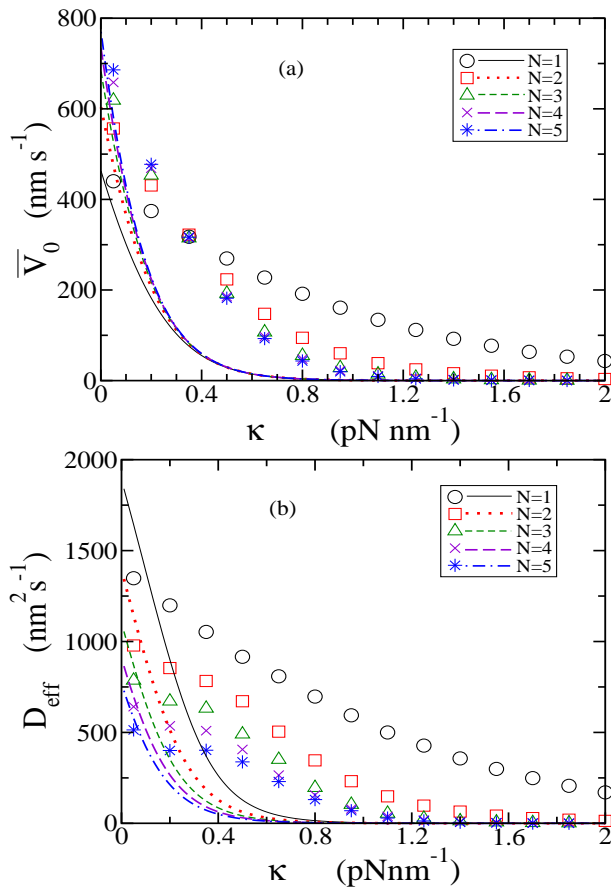


FIG. 9. (color online) Average velocity and effective diffusion coefficient of cargo for Model II is shown here for $\theta = 0.9$. All the other parameters are chosen from Table I. The deviation of analytical results (lines) from simulation (symbols) is significant in this case, compared to that in $\theta = 0.1$ case (Fig.3(b) and Fig.4(b)).

[3] F. Julicher, A. Ajdari and J. Prost, Rev. Mod. Phys. **69**, 1269 (1997).
 [4] D. Chowdhury, Phys. Rep. **529**, 1 (2013).
 [5] S. P. Gross, Phys. Biol. **1**, R1 (2004).
 [6] M. A. Welte, Curr. Biol. **14**, R525 (2004).
 [7] V. Soppina, A. K. Rai, A. J. Ramaiya, P. Barak and R. Mallik, Proc. Natl. Acad. Sci. USA **106**, 19381 (2009).
 [8] K. Furuta, A. Furuta, Y. Y. Toyoshima, M. Amino, K. Oiwa and H. Kojima, Proc. Natl. Acad. Sci. USA **110**,

501 (2013).
 [9] E. B. Stukalin, H. Phillips III and A. B. Kolomeisky, Phys. Rev. Lett. **94**, 238101 (2005).
 [10] E. B. Stukalin and A. B. Kolomeisky, Phys. Rev. E **73**, 031922 (2006).
 [11] A. Kunwar, M. Vershinin, J. Xu and S. P. Gross, Curr. Biol. **18**, 1173 (2008).
 [12] D. Materassi, S. Roychowdhury, T. Hays and M. Salapaka, BMC Biophys. **6**, 14 (2013).
 [13] A. Kunwar *et al*, Proc. Natl. Acad. Sci. USA **108**, 18960 (2011).
 [14] F. Berger, C. Keller, S. Klumpp, and R. Lipowsky, Phys. Rev. Lett. **108**, 208101 (2012).
 [15] F. Berger, C. Keller, R. Lipowsky, S. Klumpp, Cellular and Molecular Bioengineering **6**, 48 (2013).
 [16] S. Bouzat and F. Falo, Phys. Biol. **7**, 046009 (2010).
 [17] S. Bouzat and F. Falo, Phys. Biol. **8**, 066010 (2011).
 [18] N. G. van Kampen, *Stochastic Processes in Physics and Chemistry* (Elsevier, Amsterdam, 2007).
 [19] J. W. Driver, A. R. Rogers, D. K. Jamison, R. K. Das, A. B. Kolomeisky and M. R. Diehl, Phys. Chem. Chem. Phys. **12**, 10398 (2012).
 [20] S. Klumpp and R. Lipowsky, Proc. Natl. Acad. Sci. USA **102**, 17284 (2005).
 [21] M. J. Müller, S. Klumpp and R. Lipowsky, Proc. Natl. Acad. Sci. USA **105**, 4609 (2008).
 [22] R. J. Glauber, J. Math. Phys. **4**, 294 (1963).
 [23] M. Einax, M. Korner, P. Maass and A. Nitzan, Phys. Chem. Chem. Phys. **12**, 645 (2010).
 [24] M. E. Fisher and A. B. Kolomeisky, Proc. Natl. Acad. Sci. USA **96**, 6597 (1999).
 [25] T. Schmiedl and U. Seifert, Eur. Phys. Lett. **83**, 30005 (2008).
 [26] D. Bhat and M. Gopalakrishnan, Phys. Biol. **9**, 046003 (2012).
 [27] R. Mallik, B. C. Carter, S. A. Lex, S. J. King and S. P. Gross, Nature **427**, 649 (2004).
 [28] A. K. Rai, A. Rai, A. J. Ramaiya, R. Jha, and R. Mallik, Cell **152**, 1 (2013).
 [29] K. Visscher, M. J. Schnitzer and S. M. Block, Nature **400**, 184 (1999).
 [30] H. Dekker and N. G. van Kampen, Phys. Lett. **76A**, 101 (1980).
 [31] M. Gitterman and G. H. Weiss, Phys. Rev. E **47**, 976 (1993).
 [32] R. Grima, J. Chem. Phys. **133**, 035101 (2010).